15

Multi-Objective Optimization of a Hybrid Steam Stripper-Membrane Process for Continuous Bioethanol Purification

Krishna Gudena, Gade Pandu Rangaiah and S. Lakshminarayanan
Department of Chemical and Biomolecular Engineering,
National University of Singapore, Singapore

15.1 Introduction

Energy plays a vital role in meeting basic human needs and demands, including requirements for a sufficient quantity of good quality food, clean water, clean air, and transportation. Rapid industrialization and lifestyle changes around the world have also resulted in a continuous increase in the demand for energy. During the past few decades, sharp fluctuations in crude oil prices and rising concerns about pollution have motivated extensive searches for alternative, clean, renewable, and low-cost fuels. Increasing energy security, curbing greenhouse gas emissions, and addressing environmental and related economic concerns are therefore key considerations for many countries.

In order to address the above concerns and considering the availability of diverse lignocellulosic and non-lignocellulosic feedstocks, research in the field of bio-based fuels has been accelerating, as has its application. For example, the Biomass R&D Technical Advisory Committee of the US has envisioned 30% replacement of their petroleum consumption with biofuels by 2030 (Perlack *et al.*, 2005). Bioethanol is one of the many promising alternatives among biofuels to meet the energy demand in the future. It can be blended with

Multi-Objective Optimization in Chemical Engineering: Developments and Applications, First Edition.
Edited by Gade Pandu Rangaiah and Adrián Bonilla-Petriciolet.

gasoline and has a higher octane number and heat of vaporization than gasoline. Moreover, bioethanol is less volatile, less toxic, and can reduce the formation of photochemical smog (Wyman, 1996). Currently, Brazil and the US are the predominant producers/ users of ethanol as a biofuel, and together they contribute to nearly 90% of global bioethanol production for use as fuel (Flavin *et al.*, 2006). At present, different blends of bioethanol with gasoline are available in the market, a few of them being E5 (5% ethanol and 95% gasoline), E10, E85 and E100. Depending on the geographical location, the associated safety norms, and the type of vehicle used, ethanol is correspondingly blended with gasoline in various proportions. For example, "flexible-fuel" vehicles can run on any ratio of gasoline and ethanol, ranging from neat gasoline to neat ethanol (E100). However, due to the occurrence of cold-start problems, the maximum content of ethanol used in engines is limited during cold weather (temperatures lower than 11 °C). Bioethanol has a research octane number (RON) and a motor octane number (MON) of 109 and 90, respectively, whereas gasoline has a RON and a MON of 91–98 and 83–90, respectively (Johansson *et al.*, 1993). In addition, bioethanol can also be used in an unblended form in vehicles having dedicated engines to use neat ethanol. However, the energy density of bioethanol is two-thirds of that of gasoline, and so it has a lower fuel economy. Phase splitting, a cold-start problem, and corrosion are some of the issues associated with bioethanol.

Bioethanol is obtained from fermentation of renewable feedstocks, and the production process is a much-researched area. Feedstock may be energy crops, crop residues or waste biomass. The production process for bioethanol from lignocellulosic biomass is briefly described here, and a schematic of this is provided in Figure 15.1. Details of the complete

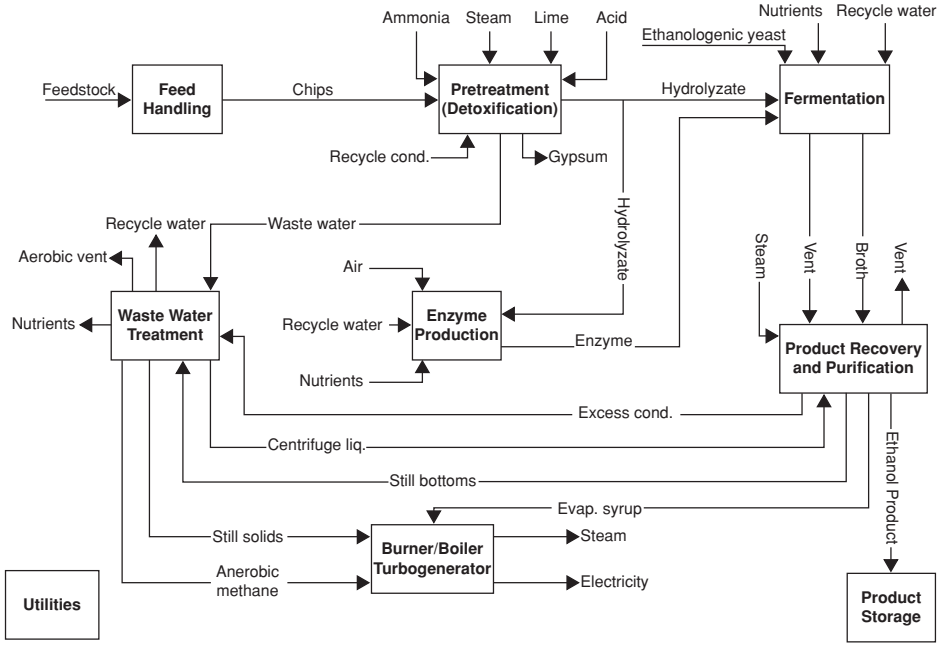

Figure 15.1 *Block diagram of bioethanol production from lignocellulosic feed (Aden* et al.*, 1999).*

process can be obtained from the technical report released by National Renewable Energy Laboratory (www.nrel.gov/docs/fy99osti/26157.pdf) (Aden *et al.*, 1999). Bioethanol production process consist of nine major steps, as follows: (i) feed handling (storage and size reduction), (ii) pre-treatment and conditioning/detoxification, (iii) simultaneous saccharification and co-fermentation, (iv) enzyme production, (v) product recovery and purification (distillation/dehydration/evaporation/scrubbing), (vi) wastewater treatment (aerobic and anaerobic digestion), (vii) lignin combustion (steam and electricity generation), (viii) product storage and (ix) other utilities.

Bioethanol produced within the fermentor in step (iii) is dilute in its concentration, generally, 1–5 wt%, and hence recovery and further purification (step v) becomes an energy- and resource-intensive task. It is observed that typically, 50–70% of the total cost of a biotechnological process comes from downstream processing (www.bioeconomy.net/reports/files/sra.pdf, accessed December 12, 2012). Different methods are practiced and discussed in the literature to recover ethanol from the fermentation broth, some of them being distillation, extraction, adsorption and membrane separation. Comprehensive literature on different kind of technologies available for bioethanol production and purification can be found in the literature (Wyman, 1996; Aden *et al.*, 1999; Huang *et al.*, 2008; Vane, 2008). Among these, distillation is the most practiced technique in industry for the purification of bioethanol, followed by adsorption. As distillation can purify up to maximum of 95.6 wt% of ethanol due to the formation of low-boiling water-ethanol azeotrope (at 1 atm), a further separation step, such as adsorption using a molecular-sieve to obtain dehydrated ethanol at higher purity, is imperative. Although the process of distillation followed by adsorption is widely applied in industry, this technology as a whole is still energy intensive (Huang *et al.*, 2010).

Recently, Huang *et al.* (2010) studied an alternative separation process by combining vapor-permeation membrane and distillation (stripper only) processes, for the economical purification of high-purity bioethanol (99.7 wt%). The hybrid stripper-membrane separation system showed substantial energy savings compared to the distillation-adsorption process (reduction by nearly half), with net savings of $3 millions/year for a typical plant producing 30 million gallons of ethanol/ year (Huang *et al.*, 2010).

Since the membrane-stripper hybrid system consists of several energy-intensive and vacuum-operated units, operation optimization of the entire separation process to obtain high purity of ethanol at minimum operating cost is highly desirable. The objective of the study described in this chapter is to formulate and optimize the hybrid stripper-membrane system for bioethanol separation. For this purpose, the process is designed in detail and realistically. Important sets of conflicting objectives, namely, (i) maximization of bioethanol purity versus minimization of operating cost (OC), and (ii) minimization of ethanol loss versus minimization of OC, are considered and solved as multi-objective optimization (MOO) problems. Pareto-optimal solutions thus obtained for these conflicting objectives are useful for better understanding of the stripper-membrane system and for selecting one of them for implementation.

The rest of this chapter is organized as follows. Section 15.2 describes the hybrid stripper-membrane system technology. Section 15.3 details MOO problem formulation for this separation system and its solution. The results obtained are presented and discussed in section 15.4. The chapter ends with conclusions and suggestions for future work in section 15.5.

15.2 Description and Design of a Hybrid Stripper-Membrane System

15.2.1 Hybrid Stripper-Membrane System of Huang *et al.*

The plant-scale design of the hybrid system by Huang *et al.* (2010) comprised several units, the major ones being a 15-stage stripper, a vacuum compressor, and a two-stage membrane unit. A schematic of this system is shown in Figure 15.2. The values of variables and system parameters shown in this figure are taken from Huang *et al.* (2010). Dilute fermentation broth from the fermentor enters the top of the stripper column, as the feed to the separation system. The stripper column with a reboiler operates under vacuum (0.5 bar), where the

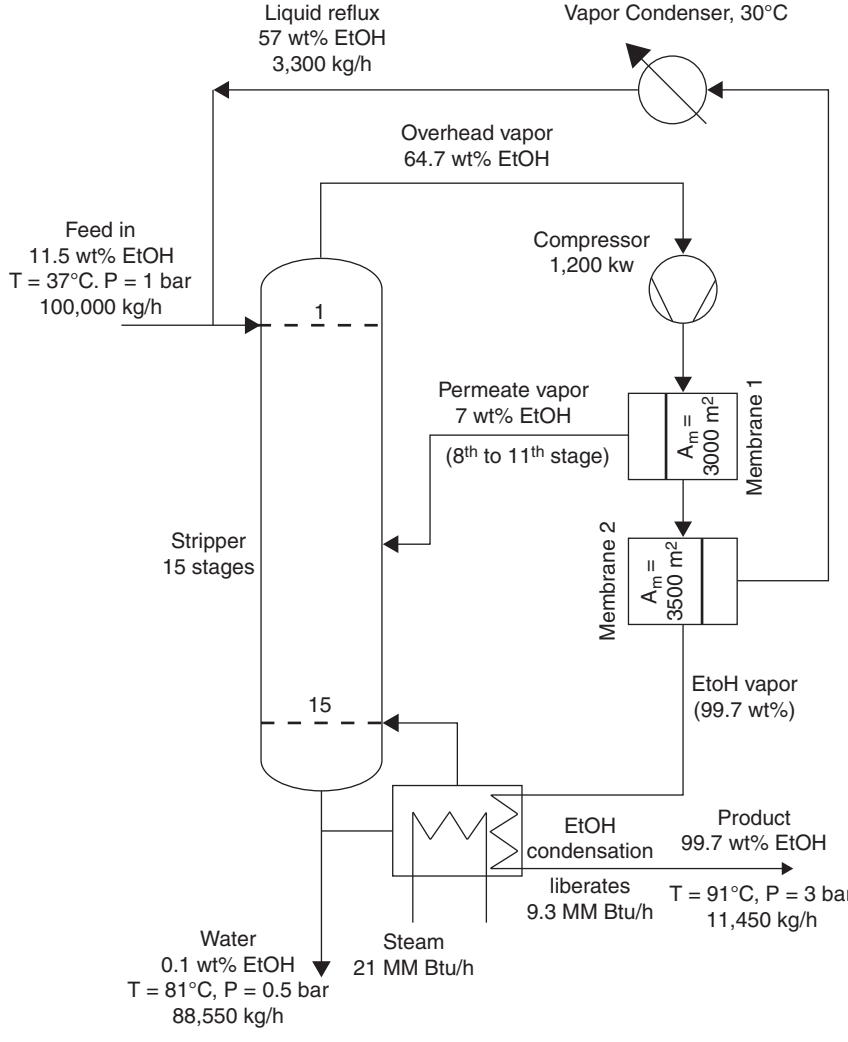

Figure 15.2 *Schematic of a hybrid stripper-membrane unit (Huang* et al.*, 2010).*

dilute broth undergoes ethanol-water separation. The overhead vapor leaving the column becomes relatively concentrated in ethanol (∼65 wt% ethanol, depending on the operating conditions), and is compressed to 3 bar.[1] Compression raises the temperature of the vapor stream, and so compressor outlet stream is cooled to a temperature of approximately 5 °C above the dew point (∼120 °C). A heat exchanger integrated with the reboiler (not shown) is used to cool this vapor stream.

The hot vapor stream then passes through a two-stage membrane vapor permeation unit, where further concentration of ethanol in the retentate takes place. The permeate stream from the membrane unit-1 (MU-1) mainly consists of water vapor, and is recycled to the stripper at between 8^{th}-11^{th} stage. The permeate stream from membrane unit-2 (MU-2) consists of relatively low water content; it is condensed and then mixed with the stream from fermentation broth as the feed to the stripper. The retentate stream from the second stage of the membrane unit consists of ethanol of desired purity. It undergoes vapor condensation in the stripper reboiler to provide heating, thus recovering the latent heat from the product stream. As this is insufficient, steam is used to supply the remaining energy for vaporizing water in the reboiler.

15.2.2 Modified Design of the Hybrid Stripper-Membrane System

The proposed flowsheet by Huang *et al.* (2010) was designed under certain assumptions. In order to model and optimize the hybrid stripper-membrane process with high fidelity, several important factors have been implemented in the present study. Figure 15.3 shows the modified flowsheet, and the corresponding major changes are discussed below. Lignocellulosic ethanol is generally of very low concentration, in the range from 1–5 wt%. On the other hand, the concentration of corn-based ethanol from the fermentor is typically high (as high as 15 wt%). For this study, mildly concentrated feed, namely, ethanol at 11.5 wt% was considered for consistency with the study by Huang *et al.* (2010).

1. Adiabatic thermal efficiencies of vacuum compressors and above-atmospheric compressors were significantly different. A multi-stage compressor with realistic efficiencies (Ryans and Bays, 2001) and intermediate cooling was implemented.
2. Instead of an equilibrium-based approach, a rigorous rate-based column simulation was performed using interface-based mass transfer rates to obtain accurate results.
3. The Aspen Plus inbuilt correlation for bubble-cap trays was chosen to calculate the pressure drop across the column. A pressure drop of 0.1 bar and 0.2 bar was assumed for coolers and reboiler respectively (Turton *et al.*, 2009), and a pressure drop of 0.02 bar was assumed for the "vapor condenser" after "membrane 2" (Figure 15.3).
4. According to Huang *et al.* (2010), the permeate vapor stream from MU-2 has to be cooled to 30 °C to completely condense and create spontaneous vacuum conditions on

[1] Heuristics state that it is often more economical to condense a vapor stream, pump it to the required pressure, and vaporize it again, than to directly compress the vapor stream. This particular heuristic was analyzed by performing simulations in Aspen Plus. It is found that, depending on the steam and electricity costs, compression of the vapor stream leaving the stripper can be economical or expensive compared to the condensing-pumping-reheating procedure. For example, Turton *et al.* (2009) provide steam and electricity costs that are comparable per unit of energy supplied. However, this may not be the case always; for example, steam cost in Seider *et al.* (2010) is nearly four times cheaper than that in Turton *et al.* (2009) whereas the electricity cost is same in both the references ($0.06/kWh). The particular heuristic is also strongly dependent on the compressor efficiency that affects its energy requirement. For this study, utility costs from Turton *et al.* (2009) have been used, and the cost analysis with this data showed that compressing the vapor stream is more economical than the condensing-pumping-reheating procedure.

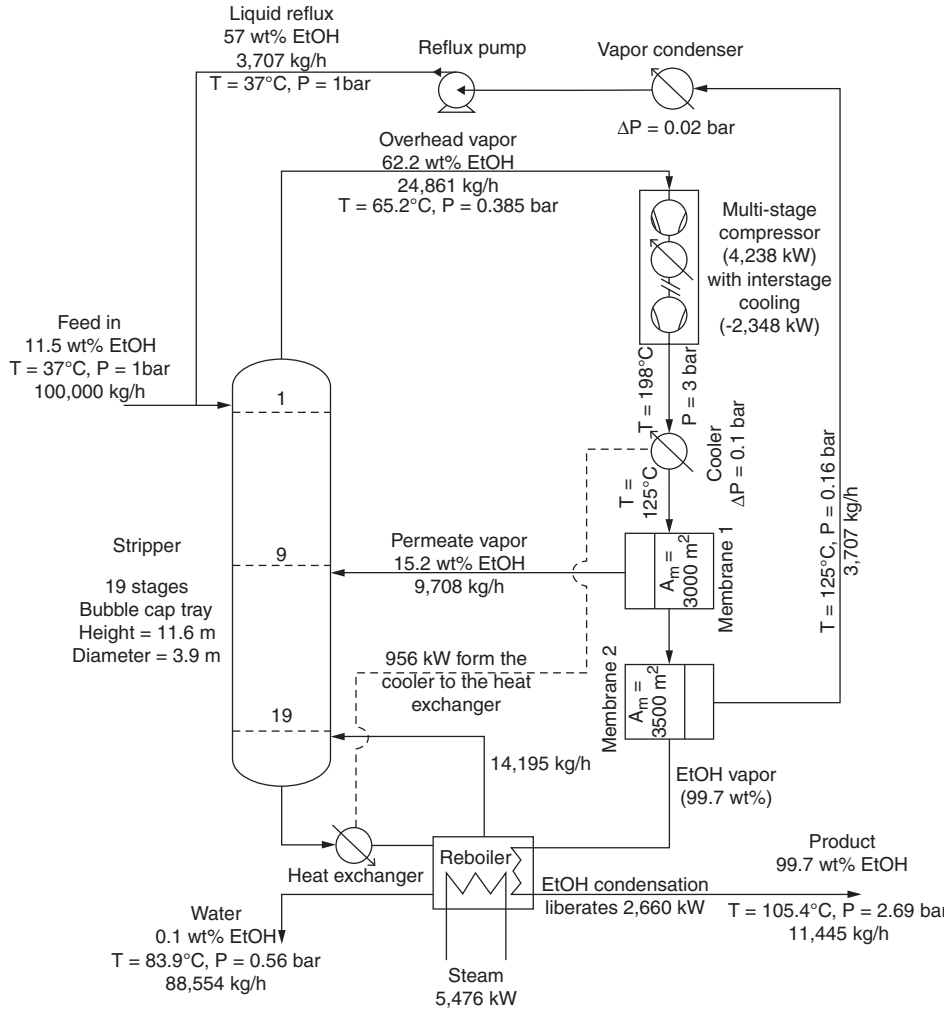

Figure 15.3 *Modified schematic of a hybrid stripper-membrane unit. The data shown in the figure is for the particular optimized case of 99.7 wt% of ethanol purity in the product stream and 0.1 wt% of ethanol loss at the stripper bottoms.*

the permeate side. However, cooling water available in industries is generally in the temperature range of 27–32 °C. Considering a ΔT_{min} of 10 °C for the condenser in Huang *et al.*, cooling water temperature has to be at a temperature of 20 °C, which may not be available in many locations throughout the year. Hence, cooling/condensation of the permeate stream from the second stage of the membrane unit was constrained to a maximum of 37 °C in order to create a spontaneous vacuum. A minimum temperature driving force (ΔT_{min}) of 10 °C and 15 °C for coolers and reboiler, respectively, is now considered.

5. The permeate stream of the MU-2 was at 0.1 bar; it was condensed and then returned to the stripper operating at 0.5 bar. Hence, a pump was included to raise the pressure of the condensed stream to atmospheric pressure.

15.2.2.1 Process Design and Simulation in Aspen Plus

The thermodynamic property package, and the design and configuration of the important units implemented in the Aspen Plus simulation software are discussed in this section. Selection of a suitable thermodynamic property package to predict the vapor-liquid equilibrium for the studied components is important, as it can affect the simulation results considerably. The non-random two-liquid model (NRTL) property method in Aspen Plus is generally recommended for non-ideal components in the ethanol-water system, and hence chosen for calculating activity coefficients for liquid-phase mixtures. The vapor phase is represented by the ideal gas equation of state. The simulation file for 99.7 wt% ethanol purity case (as outlined in Figure 15.3) is made available for the academic usage in the CD of this book.

15.2.2.1.1 Column Simulation: To simulate the column within Aspen Plus, either the equilibrium-based approach or the rate-based approach can be implemented. The former approach considers the liquid and vapor streams leaving a tray to be in equilibrium; and a large set of nonlinear equations arising from mass balances, phase equilibrium relations, mole fraction summations, and energy balances are solved. However, in reality, the liquid and vapor streams leaving a tray are unlikely to be in equilibrium, and this is accounted in the equilibrium-based model via an efficiency factor. On the contrary, the rate–based approach is closer to reality as it performs rigorous multi-component mass and heat transfer-rate modeling, where equilibrium is assumed to be established at interface only. The interface mass transfer rate for the multi-component system is obtained from the Maxwell–Stefan theory.

Aspen Plus has both the rate-based and equilibrium-based models in its Radfrac unit. Ethanol-water separation simulation within the stripper is implemented in this study, based on the rate based-model. The simulated column comprises 20 stages (19 stages with bubble cap trays and reboiler). The feed enters the top stage (stage 1) of the stripper, and the recycle stream from the MU-2 enters at stage 1 of the column. Aspen Plus provides an RADFRAC module to simulate columns. This was used in this study. The documentation in RADFRAC states that the stage counting starts from the condenser (stage 1) and ends at the reboiler. However, in the absence of a condenser, stage 1 is the first plate. The top-stage pressure of the column is specified as 0.5 bar as an initial guess. Mass and heat transfer coefficients on bubble cap trays were calculated, within Aspen Plus, using the AIChE (1958) correlation and the Chilton and Colburn method, respectively. Scheffe and Weiland's (1987) approach was selected to calculate the interfacial area.

An estimate of the column diameter is needed to simulate it using the rate-based approach. For this purpose, the column is first simulated using the equilibrium-based approach and the diameter value from the sizing results is obtained. Note that a constant column diameter is assumed in all the MOO runs. For this purpose, the column dimension has to be such that it is valid over the entire range of decision variables to avoid any possibility of flooding. Thus, the column diameter obtained from the equilibrium-based model was used to set its value at 3.87 m for all simulations during MOO. The tray spacing was set at the default value of 0.6096 m. Bulk properties for each phase on each stage are needed to evaluate the corresponding energy and mass fluxes. These were calculated by selecting mixed-flow

model in the rate-based approach, which assumes that bulk property for each phase on any given stage is equal to the property of the stream leaving that stage.

15.2.2.1.2 Membrane Configuration: The overhead vapor leaving the stripper is compressed to a maximum of 3 bar. Compression results in a temperature increase, and the stream has to be cooled near to its dew point. The operating temperature of the membrane is thus maintained at 128 °C, which is ∼5 °C above its dew point to prevent condensation. According to Huang *et al.* (2010), the challenge here is the availability of membranes that can sustain high operating temperatures (120–130 °C), and they stated that Membrane Technology and Research (MTR) and the US Environmental Protection Agency (USEPA) have developed such membrane modules. Water-permeable materials such as cross-linked hydrophilic polymers and hydrophobic perfluoropolymers have been used by them to develop related composite membranes. The water and ethanol permeance values for the simulated membrane unit is 2000 gpu and 50 gpu, respectively (Huang *et al.*, 2010); note that one gas permeation unit (gpu) is 10^{-6} cm^3(STP)/(cm^2.s.cm Hg). The vapor-permeation membrane area assumed in Huang *et al.*'s study was 2000 m^2 and 2500 m^2 for the first and second units, respectively. However, due to the occurrence of infeasible solutions when targeting high ethanol purity during MOO, membrane area was increased to 3000 m^2 and 3500 m^2, respectively, in the present study.

15.2.2.1.3 Membrane Module Modeling: The permeate side of the membrane is maintained at vacuum, and vapor permeation is the underlying phenomenon for the transport and separation of components. A vapor-permeation membrane module is unavailable readily in the Aspen Plus User Interface. However, Aspen Custom Modeler has an inbuilt code for the gas-permeation module, and it can be imported into Aspen Plus User Interface. The following are the underlying assumptions for the membrane model used in this work.

1. Transport phenomena across and along the vapor permeation membrane module can be adequately represented by discretizing them and solving as a set of multiple cells. Here, the default value of $N_{cells} = 100$ was used.
2. A cross-flow mechanism with unhindered permeate withdrawal (permeate is removed from each cell and mixed to form the module permeate) and retentate flow from one cell to the next is assumed.
3. A constant temperature exists along the interior of the entire membrane module.
4. The vapor stream follows ideal gas behavior.
5. Constant permeability of components (ethanol and water) is assumed for the given process conditions.

15.2.2.1.4 Compressor Configuration and Design: Adiabatic thermal efficiency of compressors is an important factor for estimating the energy needed for compression. For a process gas compressed from initial pressure (P_{in}) to final pressure (P_{out}), it is defined as:

$$\eta_{compressor} = \frac{\text{Theoretical adiabatic horsepower}}{\text{Actual brake horsepower}} \tag{15.1}$$

Efficiencies of vacuum compressors are significantly lower than compressors that operate above atmospheric pressure. Typically, compressors operating above atmospheric pressure have an efficiency of 0.7–0.8 (Turton *et al.*, 2009) whereas dry vacuum pumps have low thermal efficiencies and vary over a wide range. Depending on the operation pressure and

the type of dry vacuum-pump used, adiabatic thermal efficiency can vary from 0.01 to 0.5 (Ryans *et al.*, 2001). In this work, three-stage screw compressors with interstage cooling are used to keep temperature below 204 °C (Turton *et al.*, 2009), and the corresponding efficiencies and discharge pressures are as follows:

1. Screw compressor 1: $\eta_{compressor} = 0.33$; discharge pressure = 0.63 bar (fixed).
2. Screw compressor 2: $\eta_{compressor} = 0.33$; discharge pressure = 1 bar (fixed).
3. Screw compressor 3: $\eta_{compressor} = 0.75$; discharge pressure = 3 bar (initial guess).

Lower adiabatic efficiencies, for compression below atmospheric pressure result in a drastic increase in energy for compression, increased release of heat and high exit-gas temperature. A rigorous multi-stage polytropic compressor using ASME method is chosen from Aspen Plus to model the compression system in the hybrid stripper-membrane system. The mechanical efficiencies for all the compressors were specified as 0.95.

Due to various operation and design constraints (for example, material of construction), intermediate cooling in a multi-stage compression is generally desirable and implemented here so that the outlet temperature from any of the compressors does not rise above 204 °C (Turton *et al.*, 2009). To meet this constraint, the outlet temperatures of the first, second, and third coolers are specified as 80 °C, 95 °C and 125 °C, respectively. The reason behind selecting such high temperatures is to prevent liquid formation at the inlet to the next compressor or membrane unit. A pressure drop across each of the coolers is assumed to be 0.1 bar (Turton *et al.*, 2009).

15.3 Mathematical Formulation and Optimization

The applicability and benefits of MOO are studied for conflicting objectives in a hybrid stripper-membrane system. Two important scenarios, each consisting of two conflicting objectives, are examined: (A) maximize ethanol purity ($\boldsymbol{f_{purity}}$) and minimize operating cost per kg of product ($\boldsymbol{f_{cost}}$), and (B) minimize ethanol loss per kg of product ($\boldsymbol{f_{loss}}$) and minimize $\boldsymbol{f_{cost}}$. Chemical engineers can see the conflicting nature of the objectives in each of these scenarios. MOO provides quantitative results on the tradeoff among the objectives involved and many optimal solutions including values of decision variables.

Case A: Maximize Ethanol Purity (f_{purity}) and Minimize Operating Cost per kg of Product (f_{cost})

The study of ethanol purity ($\boldsymbol{f_{purity}}$), as one of the objectives, is important for two main reasons; firstly, the separation of most of the water from the bioethanol is necessary as its presence above a certain limit may result in phase separation when mixed with gasoline, especially at low temperatures. Contamination of a gasoline-ethanol mixture by water may also result in corrosion of metal parts and reduced fuel performance. In addition, due to the hygroscopic property of ethanol, there is a maximum safety limit. One of the hurdles for bioethanol distribution is the lack of common consensus on the limits for water in the fuel. The American Society for Testing and Materials (ASTM) specification for water in ethanol is 1.3 wt% and the specification according to European Union standards (EN 15376) is 0.3 wt% (D4806-04a, 2004; Vane, 2008). Secondly, bioethanol-dedicated engines in vehicles that run on neat alcohol (E100) allow hydrous ethanol, which has a higher octane

number and a good anti-knocking property. Hence, wt% of water in bioethanol and the corresponding OC may vary for different production scenarios.

Knowledge on the tradeoff between purity and OC will therefore be of economic interest. The Pareto-optimal solutions obtained from MOO will help decision-makers to identify the extra OC (if any) incurred in purifying bioethanol to a higher target level. The solutions will also provide quantitative insights on the competitiveness of the studied membrane-stripper technology for bioethanol purification.

Case B: Minimize Ethanol Loss (f_{loss}) and Minimize Operating Cost per kg of Product (f_{cost}) The separation efficiency for a system is generally described by its ability to achieve desired purity with minimal loss of the product (here, bioethanol) in the waste stream (stripper bottoms); this will also reduce the wastewater treatment cost. However, reduction in product loss is likely to increase OC. Simultaneous minimization of OC and ethanol loss per unit of product is therefore of interest.

15.3.1 Problem Formulation

The MOO problem for bioethanol purification by hybrid membrane-stripper system for Case (A) can be formulated as shown below.

$$\begin{aligned}
&\text{Maximize} && \text{Ethanol purity, } f_{purity}\,(\%) && (15.2)\\
&\text{Minimize} && \text{Operating cost per kg of product, } f_{cost}\,(\$/\text{kg}) && (15.3)\\
&\text{subject to} && P_{mem,1} \geq P_{col,\,stage1} + 0.1\,bar && (15.4)\\
& && T_{condenser,out} \geq 37^{\circ}C && (15.5)\\
& && \mathrm{T}_{cooler,out} \geq T_{stage,19} + 10^{\circ}C && (15.6)\\
& && T_{product} \geq T_{reboiler} + 15^{\circ}C && (15.7)\\
& && Ethanol_{\,bottoms}\,wt\% = 0.1 && (15.8)
\end{aligned}$$

In addition to the above, model/governing equations for each and every unit must be satisfied. This is ensured by simulating the process system in a simulator such as Aspen Plus.

Equation (15.4) specifies that the permeate side pressure of the MU-1 ("Membrane 1" in Figure 15.3) should be at least 0.1 bar above the stripper operating pressure (stage 1), to ensure driving force for permeate flow into the column. The outlet temperature of the condenser is specified to be greater than 37 °C in Equation (15.5), in order to use cooling water at about 27°C. Vapor stream leaving the third stage of the compressor would be at a high temperature, and the energy from its cooling is used in the "heat exchanger" to heat the liquid stream leaving nineteenth stage of the stripper (Figure 15.3). For this, Equation (15.6) is to ensure the minimum temperature driving force (ΔT_{min}) of 10 °C. Equation (15.7) is to maintain a ΔT_{min} of 15 °C for the heat exchange of the retentate from MU-2 with the reboiler (stage 20) of the stripper. Finally, Equation (15.8) is the design specification for ethanol content in the stripper bottoms. Ethanol purity at the bottoms in Equation (15.8) can be specified as an inequality constraint as $Ethanol_{\,bottoms}\,wt\% \leq 0.1$. However, specifying the constraint in such a way in Aspen Plus results in different values of ethanol purity at the bottoms of the stripper (i.e., less than 0.1 wt%) for different runs of optimization.

Hence, to keep the ethanol purity the same in all MOO runs, it is set as an equality constraint.

Decision variables for optimization are: operating pressure for stripper ($P_{stripper}$), outlet pressure for the third stage of the compressor ($P_{compressor,3}$), permeate side pressure of MU-1 ($P_{mem,1}$), permeate side pressure of MU-2 ($P_{mem,2}$), and reboiler duty of stripper ($Q_{reboiler}$). Selection of an appropriate range of decision variables is an important step in the formulation of an optimization problem. The bounds for the decision variables for the hybrid stripper-membrane process were obtained by simulating the process by varying each of the variables within a physically meaningful range. This analysis helps to identify any difficulties in simulating the process during MOO, and is particularly useful when process simulators are used in order to avoid later difficulties. Further, bounds were set such that they cover the values used by Huang *et al.* (2010).

The lower bound for the stripper pressure ($P_{stripper}$) in Equation 15.9 was decided such that temperature rise at the outlet of the first stage of the compressor would not exceed 204 °C. As discussed in section 15.2.2.1, a three-stage compressor was used for this study. As the overhead vapor stream would be brought to at least the atmospheric pressure, the first and second stage outlet pressures were fixed at 0.63 bar and 1 bar, respectively. The third-stage compressor outlet pressure ($P_{compressor,3}$) can be varied; the range for $P_{compressor,3}$ was limited to 3 bar in Equation 15.10 below, to avoid violating the operational limit of 204 °C on the outlet temperature at the compressor exit (Turton *et al.*, 2009) during MOO. The lower bound of the permeate side pressure ($P_{mem\text{-}1}$) of MU-1 is set higher by 0.1 bar (Equation 15.11) over the lower bound of $P_{stripper}$, such that Equation 15.4 holds valid.

Permeate side pressure for MU-2 was kept above 0.1 bar (Equation 15.12) due to the practical constraints on the operation of the membrane (Huang *et al.*, 2010). Reboiler duty was limited to a maximum value of 13.96 MW (Equation 15.13) to avoid any column operational problems such as flooding or dry trays. Figure 15.3 shows energy integration (1) between "cooler" and "heat exchanger", and (2) by ethanol vapor condensation in the reboiler of the stripper. To avoid computational problems in the simulation of the process for a large range of decision variables, the process flowsheet is simulated without the energy integration. Then, the recovered energy from the two streams (from cooling and from condensation in reboiler) is deducted from the reboiler duty to calculate the total steam cost. Hence, the decision variable in Equation 15.13 below is the total reboiler duty.

In summary, bounds on decision variables are as follows:

$$0.25\,\text{bar} \leq P_{stripper} \leq 0.6\,bar \tag{15.9}$$

$$1.5\,bar \leq P_{compressor,3} \leq 3\,bar \tag{15.10}$$

$$0.35\,bar \leq P_{mem,1} \leq 1\,bar \tag{15.11}$$

$$0.1\,bar \leq P_{mem,2} \leq 0.5\,bar \tag{15.12}$$

$$5.82\,MW \leq Q_{reboiler} \leq 13.96\,MW \tag{15.13}$$

Problem formulation for Case B is similar to Case A with the following modifications. Equation (15.2) is replaced by Equation (15.14):

$$\text{Minimize} \quad \text{Ethanol loss, } f_{loss}\,(\%) \tag{15.14}$$

$$\text{Minimize} \quad \text{Operating cost per kg product, } f_{cost}\,(\$/kg) \tag{15.15}$$

Constraint in Equation (15.8) is replaced by the ethanol purity requirement:

$$Ethanol_{\,product}\; wt\% = 99.7 \tag{15.16}$$

All other constraints and decision variables are the same as those in Case A, from Equations 15.4–15.7 and 15.9–15.13. The two objectives, $\boldsymbol{f_{loss}}$ and $\boldsymbol{f_{cost}}$ with their corresponding constraints are solved simultaneously such that 99.7 wt% of bioethanol in the product stream, specified as an equality constraint in Equation (15.16), is also met.

15.3.2 Optimization Methodology for MOO Problems in Cases A and B

The ε (epsilon) constraint method suggested by Haimes *et al.* (1971) is employed in the present study to obtain the Pareto-optimal solutions. In this method, one of the objective functions in the MOO problem is chosen as the only objective (in this case, $\boldsymbol{f_{cost}}$) and the others (in this case, $\boldsymbol{f_{purity}}$ or $\boldsymbol{f_{loss}}$) are transformed into constraints using suitable values so that the transformed objectives are kept within acceptable values. The value of the objective transformed into a constraint (i.e., ε) is to be determined based on *a priori* knowledge of the system or from single objective optimization (SOO) of each objective in the MOO problem.

For example, in case B, the transformed optimization problem will be:

$$\begin{aligned}
\text{Minimize} \quad & \text{Operating cost per kg of product, } f_{cost}\ (\$/\text{kg}) && (15.17)\\
\text{subject} \quad & \text{to } f_{loss}(wt\%) \le \varepsilon && (15.18)\\
& P_{mem,1} \ge P_{\,col,stage1} + 0.1\,bar && (15.19)\\
& T_{condenser,out} \ge 37^{\circ}C && (15.20)\\
& T_{cooler,out} \ge T_{stage,19} + 10^{\circ}C && (15.21)\\
& T_{product} \ge T_{reboiler} + 15^{\circ}C && (15.22)\\
& Ethanol_{\,product}\; wt\% = 99.7 && (15.23)
\end{aligned}$$

The decision variables and their bounds for the above SOO formulation are as in Equations 15.9–15.13. One objective, $\boldsymbol{f_{loss}}$, in case B (Equation 15.14) is transformed into an inequality constraint in Equation 15.18. This additional constraint ensures that the objective, $\boldsymbol{f_{loss}}$, is less than or equal to a specific ε value. Since a higher value of $\boldsymbol{f_{loss}}$ results in a lower $\boldsymbol{f_{cost}}$, the optimizer would finally return a value of OC corresponding to $\boldsymbol{f_{loss}}$ equal to ε.

The resulting SOO problem, along with bounds on decision variables (Equations 15.9–15.13) and constraints (Equations 15.18–15.23) can be solved to obtain an optimal solution for $\boldsymbol{f_{cost}}$. In the ε-constraint method, the SOO problem is repeatedly solved for different values of ε. The optimal solutions obtained are then finally screened to find the Pareto-optimal front (i.e., non-dominated solutions).

Advantages of ε-constraint method are that: (i) it is easy to formulate and implement, (ii) it can handle problems having convex and non-convex Pareto-optimal fronts, and (iii) any single objective optimizer such as that in Aspen Plus simulator can be used. Disadvantages of ε-constraint method are: (i) its complexity increases in terms of user inputs with the increase in number of objectives, (ii) it gives only one optimal solution at a time, (iii) difficult to obtain well-distributed solutions, and (iv) it is time consuming because it requires many SOO problems to be solved and use of small changes in ε to avoid missing any optimal solution. However, the ε-constraint method is used in this work because the inbuilt

optimizer in Aspen Plus can be used readily and to demonstrate this method with a process simulator.

Optimization within Aspen Plus

An inbuilt optimizer within Aspen Plus, namely, SQP-Biegler (a sequential quadratic programming algorithm) was selected as the optimization method. The convergence test option was set to "Kuhn Tucker using Hessian." Forward difference approximation was used for the derivative calculations as it is computationally less expensive. The tolerance value for each of the constraints in the MOO formulation (section 15.3.1) is set as 1×10^{-3}, and it is set as 1×10^{-5} for the objective function. A generic set of executable FORTRAN statements for calculating the OC for a given process optimization is implemented within Aspen Plus. The objective function (here, OC in Cases A and B) is automatically calculated for each set of values of decision variables given iteratively by the SQP-Biegler algorithm, until the minimum within the given bounds and constraints, is reached. SQP-Biegler is a local optimizer, and so local solutions may be obtained in different optimization runs. Hence, for each value of ε, several optimization re-runs with initial values from the optimal results of the previous run and/or different initial guess were performed, to find the optimal solutions correctly. More discussion on this is given in the next section.

15.4 Results and Discussion

15.4.1 Maximize Ethanol Purity (f_{purity}) and Minimize Operating Cost/kg of Bioethanol (f_{cost})

Figure 15.4 shows the Pareto-optimal front of non-dominated solutions (filled circles) for the two objectives, namely, minimum OC/kg of product and maximum ethanol purity. A tradeoff (conflict) exists between these two objectives. The open circles in Figure 15.4a are dominated solutions (i.e., filled circles are better than these, and so the open circles are not the correct or global optimal solutions), and they were obtained in different runs despite

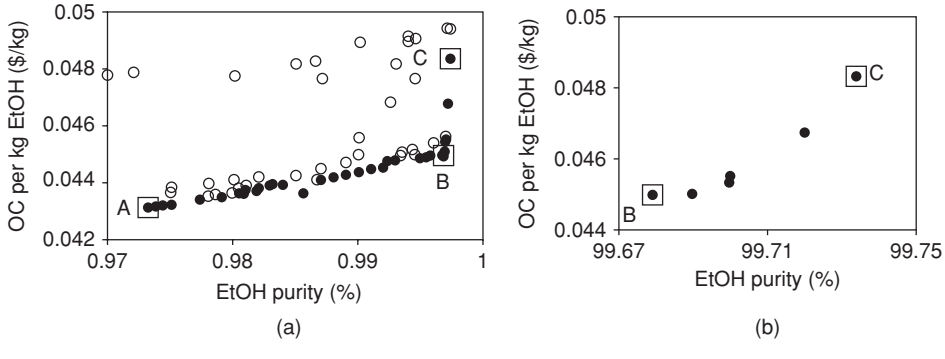

Figure 15.4 *Pareto-optimal front for the optimization of hybrid steam stripper-membrane process, in plot (a) with enlarged plot (b); dominated and non-dominated solutions are shown by open and filled circles, respectively.*

starting with good initial estimates. Possible reasons for this are: (i) the presence of multiple minima for the SOO problem, (ii) the inbuilt optimizer (SQP-Biegler) in Aspen Plus is only a local optimizer, and so can converge to a local minimum, (iii) premature convergence of the inbuilt optimizer, and (iv) the use of finite difference approximation for derivatives. Thus, it is important to run the optimizer several times for reliable and accurate results.

The Pareto-optimal solutions (filled circles in Figure 15.4a) are spread over ethanol purity from 97.33–99.73 wt% and OC/kg of product from \$0.043 to \$0.048. A steep change in the Pareto-optimal front around 99.68 wt% of ethanol purity can be seen. This implies that increase in purity beyond this value would result in rapid increase in the operating cost. Although the range of the objective $\boldsymbol{f_{cost}}$ (\$/kg) seems to be small (i.e., less than 1 cent per kg of ethanol), OC for a typical plant capacity of 30 million gal/yr (∼11,500 kg/h) varies from \$4.34 million/yr to \$4.87 million/yr. Utilizing the quantitative results from the Pareto-optimal front in Figure 15.4 and based on ethanol purity requirement (i.e., water in ethanol by ASTM is 1.3 wt% and by EN 15376 is 0.3 wt% (D4806-04a 2004; Vane 2008)), one of the non-dominated solutions and the corresponding decision variables (Figure 15.5) can be chosen.

The desired separation of an ethanol-water mixture is achieved here by hybridizing the benefits of a stripper and membrane separation. This implies that both reboiler duty (related to stripper separation) and compressor power (related to membrane separation) can be varied to obtain a target purity level for bioethanol at the lowest OC. The reboiler requires steam (in this case, low-pressure steam, LPS) whereas the compressor requires electric power. The cost of LPS (at 5 bar and 160 °C) and electric power for this study are \$27.7/ton and \$0.06/kWh, respectively (Turton *et al.*, 2009). Hence, depending on the bioethanol plant location and the prevailing cost of LPS and electricity, the MOO results in Figures 15.4 and 15.5 can vary.

The optimal values of the column pressure, MU-1 permeate side pressure and MU-2 permeate side pressure, corresponding to the Pareto-optimal front in Figure 15.4 are shown in Figure 15.5a, 15.5c and 15.5d, respectively. A continuous, nearly linear decrease is observed for the permeate side pressure of MU-2 (Figure 15.5d). This implies that, to achieve high ethanol purity in the range of 97.4 wt% to 99.68 wt% at low OC/kg product, lowering the permeate side pressure of MU-2 is most economical. According to the solution diffusion model, flux (J_i) of a component i across a membrane of given thickness (L) and permeability (P_m) is proportional to the partial pressure driving force, and is given by

$$J_i = \frac{P_{m,i}}{L}(p_{i,f} - p_{i,p}) \tag{15.24}$$

where $p_{i,f}$ and $p_{i,p}$ are the partial pressure of component i on the feed and permeate side, respectively. The greater the difference between pressures on both the sides of the membrane, the greater would be the partial pressure difference for a given composition. Therefore, for the same membrane area and at low permeate side pressure, a high driving force and a high component flux can be maintained. This better performance is, however, achieved by increasing the cost of vapor condensation and pumping liquid. At very low operating pressures, the stability of the membrane can also be an important issue. The lower limit of the MU-2 permeate side pressure is reasonable and is as suggested in Huang *et al.* (2010). There is no significant and consistent variation in column pressure and MU-1 permeate side pressure for ethanol purity from 97.4 wt% to 99.6 wt% (Figures 15.5a and 15.5c).

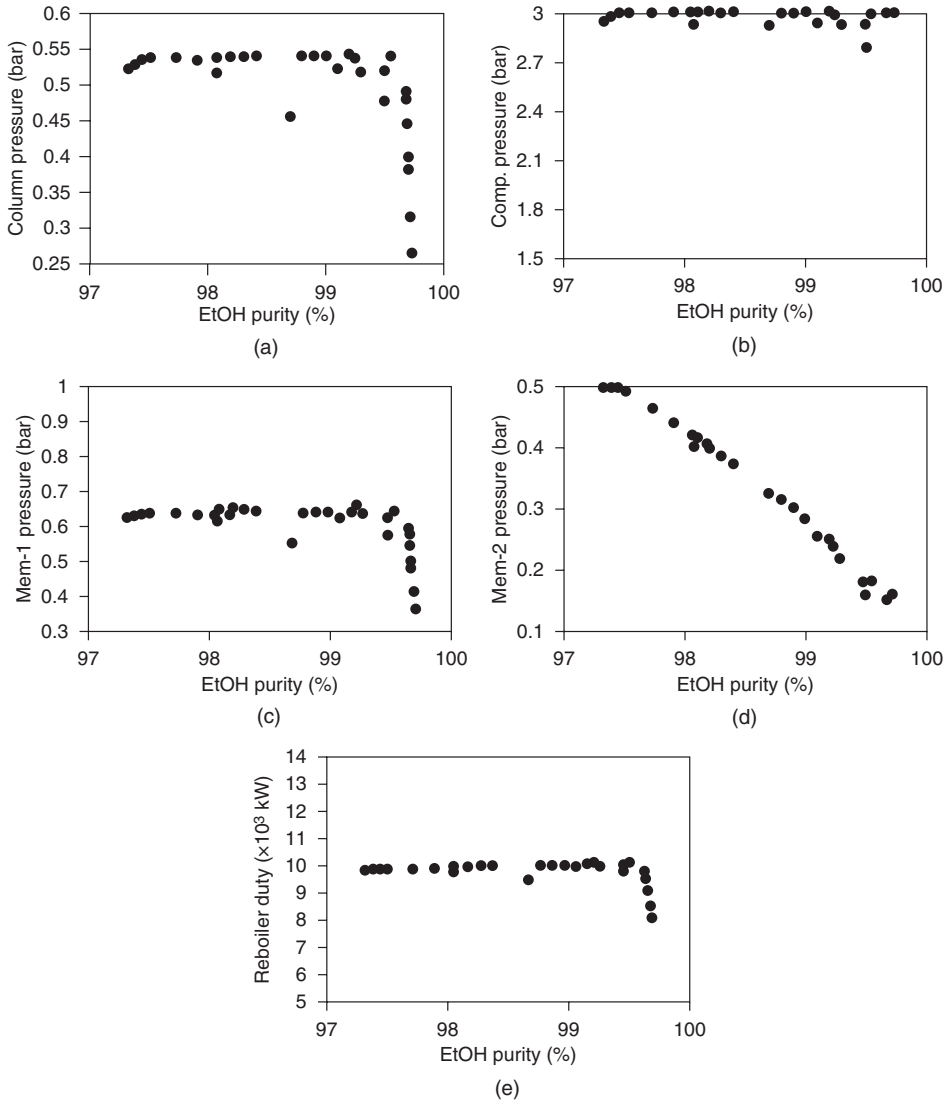

Figure 15.5 *(a) Column pressure, (b) compressor exit pressure, (c) membrane unit—1 permeate side pressure, (d) membrane unit—2 permeate side pressure, and (e) reboiler duty, corresponding to the Pareto-optimal front in Figure 15.4.*

The operating pressure of the column initially rises marginally from 0.52 bar to 0.54 bar for ethanol purity from 97.3 wt% to 97.4 wt%, and is nearly constant around 0.54 bar until ~99.6 wt%. Since permeate side of the MU-1 is related to the stripper, its variation is similar to the column pressure. In fact, it obeys the constraint in Equation 15.4 (i.e., a shift of 0.1 bar in Figure 15.5c compared to column pressure in Figure 15.5a) to provide the driving force for permeate flow to the column. However, sudden changes in the trends

in Figures 15.4, 15.5a, 15.5c and 15.5d are observed beyond 99.6 wt% of ethanol purity. MU-1 permeate side pressure and correspondingly column pressure start decreasing and nearly reaches its lower limit. The column pressure is reduced to ∼0.27 bar for ethanol purity of ∼99.74 wt%.

As discussed in section 15.2.2, spontaneous condensation of the vapor stream at the "vapor condenser" in Figure 15.3 creates the desired vacuum on the permeate side of MU-2. The temperature of the condensate leaving the "vapor condenser" (Figure 15.3) is restricted to 37 °C (Equation 15.5), and so the corresponding attainable vacuum on the permeate side of MU-2 is ∼0.16 bar. For this reason, the permeate pressure in Figure 15.5d does not go beyond ∼0.16 bar. Hence, optimization results suggest that for achieving ethanol purity beyond 99.68 wt%, the optimizer has to change MU-1 permeate side pressure. Since column pressure and permeate side pressure of MU-1 are related via Equation 15.4, reduction in the former is also observed (Figure 15.5a). Operating the column at lower pressure increases compression cost and simultaneously reduces reboiler duty (Figure 15.5e), with the net effect of increasing the objective function, OC/kg ethanol produced (Figure 15.4) for achieving ethanol purity > 99.68 wt%. Reduction in reboiler duty is observed due to the reduction in column pressure (Figure 15.5a) and, hence, corresponding enhancement in relative volatility of ethanol/water mixture.

Figure 15.5c shows the variation in the third-stage compressor exit pressure with ethanol purity. The optimal value of this decision variable is near its upper bound for the entire range of the objective function. This is to maintain high feed-side pressure to the MU-1. Some fluctuations in the compressor exit pressure are observed due to the corresponding variations in the column pressure (Figure 15.5a).

Table 15.1 shows the comparison of three selected points from Figure 15.4a. Points A and C are the optimal solutions corresponding to the minimal and maximal ethanol purity obtained, respectively, and optimal solution B is within these two extremes with 99.68% of ethanol purity. Point B is at the limit of ethanol purity beyond which OC increases significantly (Figure 15.4a). A large change in $P_{mem,2}$ is required if the user desires to shift the target ethanol purity from 97.33 *wt%* to 99.68 *wt%*. On the other hand, major changes in $P_{stripper}$, $P_{mem,1}$ and $Q_{reboiler}$ are required if the user needs to further increase the ethanol purity from 99.68 *wt%* to 99.73 *wt%* (Table 1).

Table 15.1 *Comparison of three selected Pareto-optimal solutions shown in Figure 15.4.*

Quantity	Solution A	Solution B	Solution C
Ethanol purity, $\boldsymbol{f_{loss}}$ (*wt%*)	97.33	99.68	99.73
OC, $\boldsymbol{f_{purity}}$ ($/kg)	0.043	0.045	0.048
$P_{stripper}$ (bar)	0.524	0.480	0.267
$P_{compressor,3}$ (bar)	2.949	2.996	3.000
$P_{mem,1}$ (bar)	0.624	0.580	0.367
$P_{mem,2}$ (bar)	0.500	0.159	0.164
$Q_{reboiler}$ (MW)	9.87	9.78	8.15
Compressor power (MW)	3.26	3.51	5.54

Table 15.2 *Comparisonof three selected Pareto-optimal solutions shown in Figure 15.6a.*

Quantity	Solution X	Solution Y	Solution Z
Ethanol loss, $\boldsymbol{f_{loss}}$ (*wt*%)	0.035	0.081	0.210
OC, $\boldsymbol{f_{cost}}$ ($/kg)	0.046	0.045	0.045
$P_{stripper}$ (bar)	0.370	0.397	0.435
$P_{compressor,3}$ (bar)	3	3	3
$P_{mem,1}$ (bar)	0.470	0.497	0.535
$P_{mem,2}$ (bar)	0.161	0.161	0.160
$Q_{reboiler}$ (MW)	9.03	9.19	9.41
Compressor power (MW)	4.51	4.16	3.82

15.4.2 Minimize Ethanol Loss (f_{loss}) and also Operating Cost/kg of Bioethanol (f_{cost})

The Pareto-optimal solutions for the objectives, namely, ethanol loss in the wastewater stream ($\boldsymbol{f_{loss}}$) and OC/kg of bioethanol recovered ($\boldsymbol{f_{cost}}$) are spread over ethanol loss from 0.025–0.21 wt% and OC/kg from $0.045 to $0.046 (Figure 15.6a). Purity of the ethanol product was fixed as 99.7 wt% (Equation 15.16) in this optimization. As before, although the range of $\boldsymbol{f_{cost}}$ ($/kg) is small, for a typical plant capacity of 30 million gal/yr (~11,500 kg/h), OC varies from $4.55 million/year to $4.65 million/year. As stated earlier, one limitation of ε-constraint (and also some other methods) is the difficulty in obtaining well distributed non-dominated solutions. This can be seen in Figure 15.6a where there are no solutions between 0.05 to 0.081 wt% ethanol loss. Optimal solutions X, Y and Z in Figure 15.6a and Table 15.2 are similar to solutions A, B and C obtained for Case A in section 15.4.1.

Variation in decision variables, namely, column pressure, compressor exit pressure, MU-1 permeate side pressure, MU-2 permeate side pressure and reboiler duty, corresponding to the Pareto-optimal front in Figure 15.6a is shown in Figures 15.6b–15.6f.

To achieve high ethanol purity and low ethanol loss in the wastewater stream, permeate side pressure of MU-1 has to be a lower value. Figure 15.6d shows a slight variation in MU-1 permeate pressure from 0.47 bar to 0.54 bar for 0.025–0.21 *wt%* ethanol loss. Lower permeate pressure and hence larger pressure driving force would result in enhanced performance of MU-1 (Equation 15.17). Variation in column operating pressure (Figure 15.6b) obeys the specified constraint (Equation 15.4), with a similar trend as for MU-1 permeate side pressure (Figure 15.6d) and a shift of 0.1 bar. Operation of column at lower pressure would result in higher operating cost for the vacuum compressor, but also lower reboiler duty in the range (9.03–9.41 MW) due to the increase in relative volatility of ethanol-water mixture (Figure 15.6f).

The compressor exit pressure is near its upper bound (Figure 15.6c), to provide a larger pressure driving force, and hence increased component flux across the polymeric membrane. The specification for ethanol purity in Equation 15.16 is high (99.7 *wt%*), and so the permeate side pressure of MU-2 (Figure 15.6e) is near its lower bound to maintain a large partial pressure driving force across the membrane (refer to the discussion on Figure 15.5d in section 15.4.1). However, close observation of Figure 15.6e reveals that the permeate

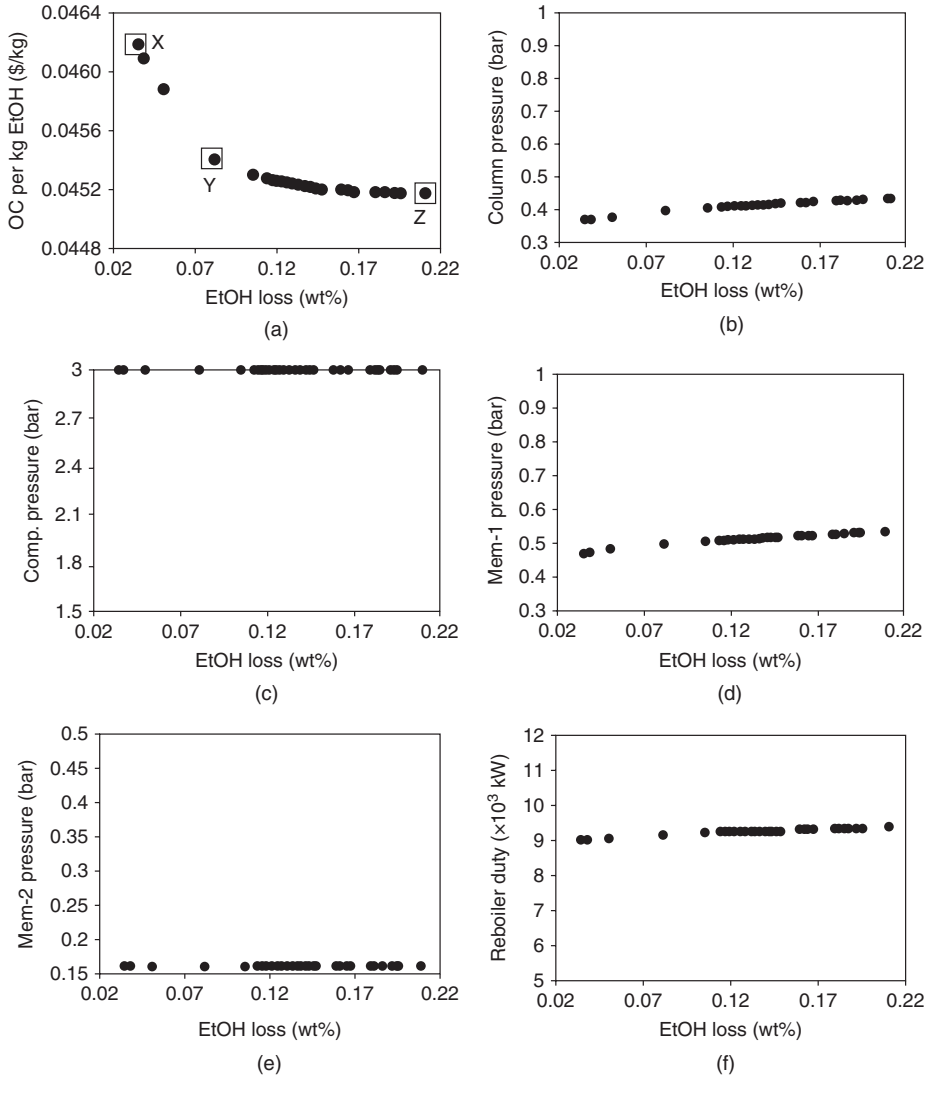

Figure 15.6 *Pareto-optimal front for the optimization of hybrid steam stripper-membrane process (plot a) and, corresponding optimal values of column pressure (plot b), compressor pressure (plot c), MU-1 permeate side pressure (plot d), MU-2 permeate side pressure (plot e), and reboiler duty (plot f).*

pressure is restricted to ∼0.16 bar. This behavior is observed due the constraint on the temperature of the condensate leaving the "vapor condenser" to 37 °C in Equation 15.5.

15.4.3 Detailed Analysis of a Selected Optimal Solution

A comprehensive analysis of one selected solution from the Pareto-optimal front in Figure 15.4 is the focus of this section. For this purpose, the optimal solution for 99.7 wt%

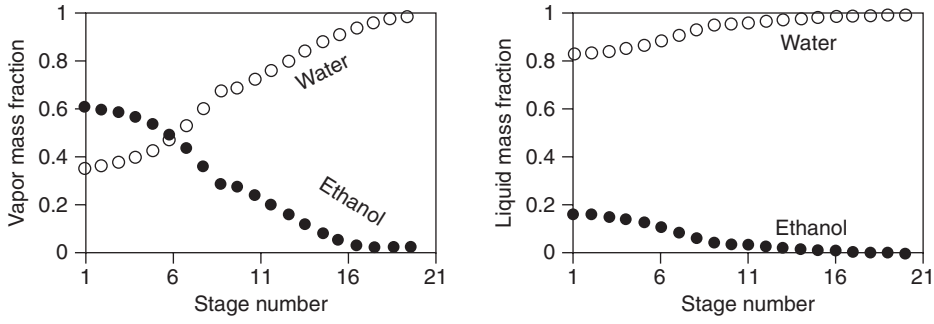

Figure 15.7 *Composition profiles of ethanol and water at different stages of the steam stripper for vapor phase (left plot) and liquid phase (right plot).*

ethanol purity in the product stream with 0.1 wt% ethanol in the wastewater stream is selected from Case A. The corresponding OC/kg product is \$0.046. For this optimal solution, the process flowsheet is given in Figure 15.3, along with the main design and operating data. Figure 15.7 shows mass fraction of water and ethanol in the liquid and vapor phases at different stages in the stripper. The concentration of water increases and ethanol decreases in both the phases from the top (stage 1) to bottom (stage 20, reboiler) of the column.

The temperature profiles of the liquid and vapor phases as well as of the vapor-liquid interface are presented in Figure 15.8. As expected, temperature increases from the top to the bottom of the stripper. The bulk liquid and vapor-liquid interface temperatures are nearly the same on all stages of the column; the maximum difference is 0.2 °C at stage 1. The vapor temperature is slightly higher than the liquid temperature. A sharp rise in vapor phase temperature is also observed at stage 9 of the stripper due to the entry of the recycle vapor at 125 °C from membrane 1.

Operating conditions at the outlet of different compressor stages and interstage coolers of the compressor system are given in Table 15.3. It can be seen that the operational constraints on temperature ($T \leq 204\,^{\circ}C$) and pressure ($P_{compressor,3} \leq 3$ bar), are within their specified range.

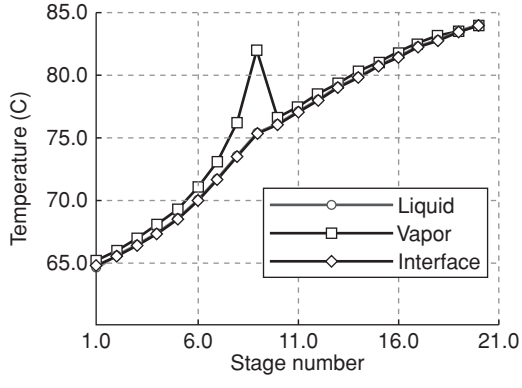

Figure 15.8 *Temperature profile at different stages of the steam stripper for liquid phase, vapor phase and vapor-liquid interface.*

Table 15.3 *Operating conditions at the outlet of the compressor stages and the inter-stage coolers of the compressor system.*

	Stage 1	Stage 2	Stage 3
Compressor			
Exit temperature (°C)	157	202.6	198
Exit pressure (bar)	0.63	1	2.99
Power (MW)	1.19	1.65	1.395
Inter-stage cooler			
Exit temperature (°C)	80	95	125[a]
Exit pressure (bar)	0.53	0.9	2.89
Vapor fraction	1	1	1

[a] This refers to the external cooler after the compressor system.

Variations in the composition of ethanol and water within the dual-stage membrane for the retentate side of the membrane are shown in Figure 15.9. The vapor stream leaving the stripper at ∼0.39 bar enters multi-stage compressor system, which increases the pressure of the inlet stream to the membrane unit to ∼3 bar. This pressurized stream with a 0.392 mole fraction of ethanol enters membrane 1 and undergoes separation within it based on the phenomenon of vapor permeation (Huang *et al.*, 2010). The composition profile (Figure 15.9) shows the performance of the first and second membrane unit (3000 m^2 and 3500 m^2, respectively). Ethanol on the retentate side is concentrated from 0.39 to 0.82 mole fraction with simultaneous decrease in water mole fraction from 0.61 to 0.18. The ethanol-water stream leaving membrane 1 is further concentrated in membrane 2, where the mole fraction of ethanol increases from 0.82 to 0.992 (equal to 0.997 mass fraction) and

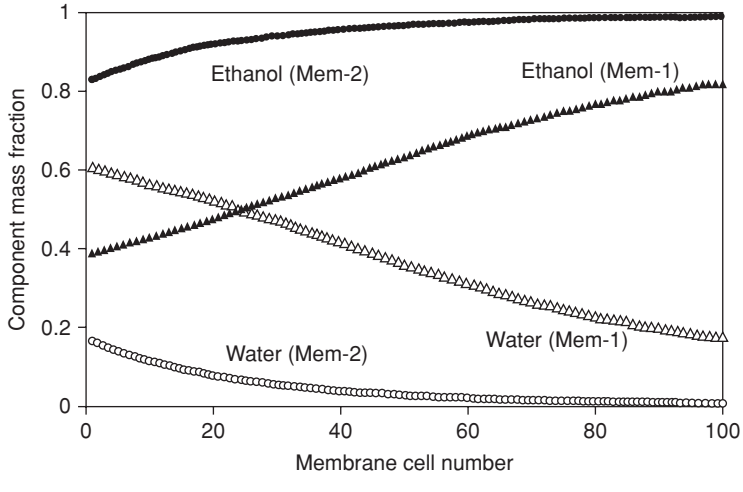

Figure 15.9 *Composition profile of ethanol and water at different discretized cells along the retentate side of the vapor permeation membranes 1 and 2.*

Table 15.4 *Energy, utilities and their costs for* $\mathbf{f_{purity}}$ *of 99.7 wt% and* $\mathbf{f_{loss}}$ *of 0.1 wt%.*

Steam	
Reboiler duty (kW)	9 092
Energy from the "Cooler" (kW)	–956
Energy from ethanol condensation (kW)	–2659
Net reboiler duty (kW)	5 477
Steam cost ($/yr)	2 293 037
Electricity	
Total compressor duty (kW)	4 238
Pump duty (kW)	0.15
Total electric power (kW)	4 238
Total electricity cost ($/yr)	2 227 500
Cooling water	
Cooling duty (vapor condenser) (kW)	–1 564
Cooling duty (multi-stage cooler) (kW)	–2 348
Total cooling duty (kW)	–3 912
Total cooling water cost ($/yr)	29 123
Total ethanol production (tons/yr)	99 960
Total OC ($/yr)	4 549 661
OC per unit bioethanol purified ($/kg)	**0.0455**

that of water decreases from 0.17 to 0.008. Thus, the desired product purity of 99.2 mole% (99.7 wt%) for the retentate stream leaving the final cell is achieved.

Table 15.4 details steam, electricity and cooling water for the selected optimal point with $\boldsymbol{f_{purity}}$ of 99.7 *wt%* ethanol. Steam (LPS) and electricity costs for the reboiler and multi-stage compressor respectively are the major contributors to the total OC for the bioethanol recovery and purification process. However, energy conservation by using the energy from cooling the compressor-exit vapor stream and from condensing ethanol vapor in the reboiler, results in ∼40% reduction in the required LPS and consequently in a major reduction in OC. Pump power is negligible (0.15 kW) compared to the compressor power (4238 kW). Cooling water is assumed to be received at 27 °C and returned at 42 °C, and its cost is taken as $0.0148/ton (Turton *et al.*, 2009). Total cooling duty for obtaining 99.7 wt% ethanol purity is –3912 kW, and the corresponding cooling water cost is $29,123/year. To summarize, for producing 99,960 tons/year of 99.7 wt% ethanol, total operating cost is ∼$4.5 million/year.

15.4.3.1 Effect of Lowering ΔT_{min} *of the "Vapor Condenser"*

From sections 15.4.1 and 15.4.2, it is observed that lowering permeate side pressure of MU-2 helps to reduce OC. However, constraint on temperature driving force (ΔT_{min}) of 10 °C for the "vapor condenser" (Equation 15.5) and cooling water temperature (section 15.2.2) in the MOO study, results in vacuum pressure on the permeate side of MU-2 being restricted ∼0.16 bar. A test case where the restriction on ΔT_{min} is reduced to 5 °C is considered. Accordingly, the constraint in Equation 15.5 is changed to $T_{condenser,out} \geq 32^{\circ}C$. The results

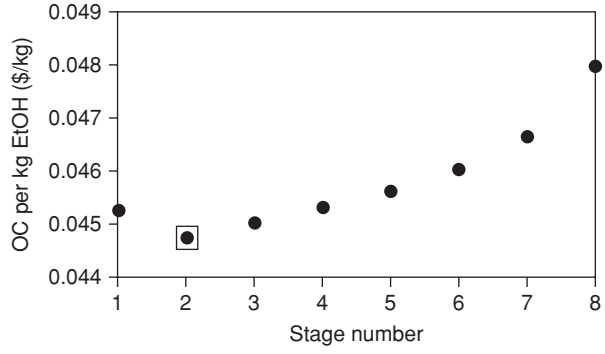

Figure 15.10 *Effect of variation in the feed stage of the column on OC/kg of ethanol ($/kg). Square box indicates the optimal feed stage location.*

(not presented here) for Case A (f_{cost} and f_{purity}) show that OC reduces marginally from \$0.0455/kg to \$0.0453/kg when ΔT_{min} for the "vapor condenser" is reduced from 10 °C to 5 °C.

15.4.3.2 Effect of Lowering the Feed Stage of the Stripper

The feed stream entering the stripper is at lower purity (11.5 *wt%* ethanol) compared to the recycle stream from the "vapor condenser" (57.7 wt% ethanol). Hence, the advantage of feeding these streams at different stages is studied using the values of decision variables obtained from the optimal solution in section 15.4.3.1 for ΔT_{min} for the "vapor condenser" as 5 °C. Figure 15.10 shows the effect of varying the feed stage on the OC/kg of ethanol. A further reduction in OC/kg ethanol can be achieved if the feed enters at the second stage of the column. The reduction in OC thus achieved is from \$0.0453/kg to \$0.0448/kg. Figure 15.11 shows the shift in the composition profiles of ethanol and water within the stripper when the feed stage (FS) is first and second.

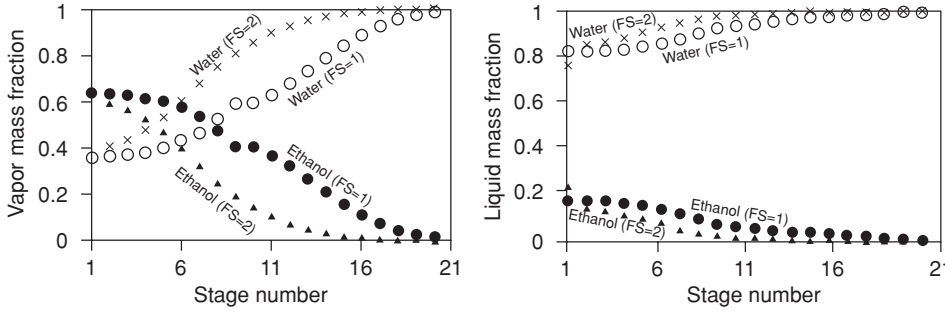

Figure 15.11 *Composition profiles of ethanol and water at different stages of the steam stripper for vapor phase (left plot) and liquid phase (right plot), for first and second feed stage (FS), respectively.*

The enhancement in the separation performance with change in the FS is clear in Figure 15.11 for many stages within the stripper. When FS is shifted from first to second, ethanol in the vapor stream leaving the top stage (stage 1) of the stripper increases from 63.6 wt% to 64.1 wt%, and ethanol in the bottoms stream from stage 20 of the stripper is reduced from 0.115 wt% to 0.0124 wt%. The reduction of ethanol in the wastewater stream results in slightly higher product flow rates (for 99.7 wt% ethanol) in the final output stream (ethanol product flow rate of 11,398 kg/h and 11,489 kg/h when FS is first and second, respectively). Hence, lowering of feed stage results in further reduction in the total OC.

15.5 Conclusions

Ethanol recovery and purification from dilute bioethanol-water mixture from fermentation using a hybrid steam stripper-membrane process is a recent and promising technology. In this chapter, the process flowsheet was first modified considering various important design and operational aspects. The application of ε-constraint method was studied with regard to its use to perform the MOO of the modified hybrid stripper-membrane process for important and conflicting objectives, namely, maximization of ethanol purity (f_{purity}), minimization of operating cost per kg of ethanol product (f_{cost}), and minimization of ethanol loss per kg of ethanol product (f_{loss}). To achieve high separation efficiency at minimum f_{cost}, permeate side pressure of MU-2 is observed to be an important handle for the optimizer. However, due to the practical limitations on cooling water temperature and ΔT_{min} of the "Vapor condenser", operation of MU-2 for permeate pressures below 0.16 bar is not feasible. This results in lowering the MU-1 permeate side pressure followed by column pressure, which increases compressor power and operating cost.

A particular case for 99.7 wt% of ethanol purity and 0.1 wt% of ethanol loss is considered to analyze various aspects of the process. The basis for selecting a particular solution from the Pareto-optimal solutions depends on criteria such as the geographical region of bioethanol use and the corresponding norms on its purity and water content in the fuel, minimum allowable loss of ethanol and the operating cost to achieve a particular separation level. Hence, the set of optimal solutions provided through this study can be used in operating the hybrid-stripper-membrane process at higher purity, less loss and lower operating cost per unit of bioethanol produced.

Developing membranes that can sustain higher temperatures and provide high permeances would help in further reducing f_{cost} for bioethanol purification. In regard to MOO, population-based techniques such as genetic algorithms, differential evolution and particle swarm optimization should be tried for obtaining the Pareto-optimal solutions. These algorithms can also be used to optimize the process for the three objectives, f_{cost}, f_{purity} and f_{loss} simultaneously, which would help in providing a holistic picture of the performance of the hybrid stripper-membrane system.

Exercises

15.1. Simulate and optimize the hybrid membrane-stripper process using the equilibrium-based approach. Compare the column performance and optimization results with those obtained using the rate-based approach in this chapter and discuss.

15.2. Perform a sensitivity analysis of the hybrid membrane-stripper process for a particular case of "99.7 wt% of ethanol purity and 0.1 wt% of ethanol loss" on operating cost per kg of ethanol, for changes in one or more of the following operational and design variables: feed flow rate, feed composition, membrane area, membrane permeance, number of stages, compressor efficiency, electricity and steam cost.

15.3. Stripper feed composition can be lower than 11.5 wt% used in this chapter. Assuming that ethanol in the stripper feed is 5 wt%, perform MOO of the hybrid membrane-stripper process for the following two cases:

(a) Case A: Maximize ethanol purity (f_{purity}) and minimize operating cost per kg of product (f_{cost}).

(b) Case B: Minimize ethanol loss (f_{loss}) and minimize operating cost per kg of product (f_{cost}).

Compare and discuss your results with those in the chapter for 11.5 wt% ethanol feed to the stripper.

References

Aden, A., Ruth, M., Ibsen, K., Jechura, J., Neeves, K., Sheehan, J., Ibsen, K., Majdeski, H., Galvez, A. (1999). Lignocellulosic Biomass to Ethanol Process Design and Economics Utilizing Co-Current Dilute Acid Prehydrolysis and Enzymatic Hydrolysis Current and Futuristic Scenarios, NREL/TP-580-26157.

D4806-04a (2004). Standard Specification for Denatured Fuel Ethanol for Blending with Gasolines for use as Automotive Spark-Ignition Engine Fuel. West Conshohocken, PA, ASTM International.

Flavin, C., Sawin, J.L., Mastny, L., Aeck, M.H., Hunt, S., MacEvitt, A., Stair, P., Podesta, J., Cohen, A.U., Hendricks, B., Mohin, T. (2006). *American Energy: The Renewable Path to Energy Security*; Worldwatch Institute; Center for American Progress, Washington, DC.

Haimes, Y., Lasdon, L., Wismer, D. (1971). On a Bicriterion Formulation of the Problems of Integrated System Identification and System Optimization. *IEEE Transactions on Systems, Man, and Cybernetics* 1(3): 296–297.

Huang, H.-J., Ramaswamy, S.T., Tschirner, U.W., Ramarao, B.V. (2008). A Review of Separation Technologies in Current and Future Biorefineries. *Separation and Purification Technology* 62(1): 1–21.

Huang, Y., Baker, R.W., Vane, Leland M. (2010). Low-Energy Distillation-Membrane Separation Process. *Industrial and Engineering Chemistry Research* 49(8): 3760–3768.

Johansson, T.B., Kelly, H., Reddy, A.K.N., Williams, R.H., Burnham, L. (1993). *Renewable Energy: Sources for Fuels and Electricity*, Island Press, Washington.

Perlack, R.D., Wright, L.L., Turhollow, A.F., Graham, R.L., Stokes, B.J., Erbach, D.C. (2005). *Biomass as Feedstock for a Bioenergy and Bioproducts Industry: The Technical Feasibility of a Billion-Ton Annual Supply*, US Department of Energy, US Department of Agriculture, Oak Ridge, TN.

Ryans, J. and Bays, J. (2001). Run Clean with Dry Vacuum Pumps. *Chemical Engineering Progress* 97(10): 32–41.

Scheffe, R.D. and Weiland, R.H. (1987). Mass-Transfer Characteristics of Valve Trays. *Industrial and Engineering Chemistry Research* 26(2): 228–236.

Seider, W.D., Seader, J.D., Lewin, D.R., Widagdo, S. (2010). *Product and Process Design Principles: Synthesis, Analysis, and Evaluation*, John Wiley & Sons, Inc., Hoboken, NJ.

Turton, R., Bailie, R.C., Whiting, W.B., Shaeiwitz, J.A. (2009). *Analysis, Synthesis, and Design of Chemical Processes*, Prentice Hall, Boston.

Vane, L.M. (2008). Separation Technologies for the Recovery and Dehydration of Alcohols from Fermentation Broths. *Biofuels, Bioproducts and Biorefining* 2(6): 553–588.

Wyman, C. (1996). *Handbook on Bioethanol: Production and Utilization*, Taylor & Francis, Washington.